Material micromachining using bursts of high repetition rate picosecond pulses from a fiber laser source

Pascal Deladurantaye, Alain Cournoyer, Mathieu Drolet, Louis Desbiens, Dany Lemieux, Martin Briand and Yves Taillon
INO, 2740 Einstein Street, Quebec City, Quebec, Canada, G1P 4S4

ABSTRACT

In this paper, we demonstrate the benefits of using bursts of picosecond pulses for material micromachining and compare the results with those obtained when using a nanosecond source with similar pulse energy, pulse width and pulse shape. The picosecond laser source used for the experiments was delivering 60-ps pulses at a repetition rate of 1.8 GHz, grouped within arbitrarily-shaped bursts having a width that could be varied from 2.5 to 40 ns. The laser output central wavelength was at 1064 nm and the output beam M^2 value was below 1.15. Micro-milling experiments were performed on silicon for two levels of energy per burst and with different burst amplitude profiles. We show that the maximum material removal efficiency and the surface quality can be increased by more than 25% when using bursts of picosecond pulses with respect to nanosecond pulses with similar energy per pulse. Effect of shaping the burst envelope of the picosecond laser on the maximum material removal efficiency is also presented.

Keywords: Laser Micromachining, Picosecond, Bursts, Micro-milling, Fiber laser, Repetition rate, Nanosecond, Shape.

1. INTRODUCTION

Since many years laser material micromachining processes have been developped using femtosecond, picosecond and nanosecond laser sources. In general different physical mechanisms can dominate a process depending on the pulse duration and on the peak intensity on the target, resulting in different regimes of material removal with corresponding yields and processing qualities[1]. Recently[2], laser ablation of metals using bursts of picosecond pulses has been investigated as a route to increase the material removal efficiency with respect to picosecond or femtosecond pulses while minimizing the increase of the Heat Affected Zone (HAZ) that limits the performances of processes relying on longer, nanosecond pulses. Further, we recently presented results showing the benefits of controlling the pulse amplitude profile in the nanosecond regime for the micro-milling of metals[3,4]. Flexible pulsed fiber laser sources having a MOPA configuration are emerging as alternatives to traditional DPSS Q-switched lasers for developing advanced laser processes in various technical fields. The possibility of controlling the pulse characteristics (rise time, width, temporal shape, and repetition rate) with a great precision and in a straightforward manner allows for exploring new laser processing capabilities using a single laser source. MOPA pulsed fiber sources can be designed to operate at high repetition rates with narrow line widths and excellent beam quality, making them suitable sources for applications like memory repair, solar cell micromachining and micro-milling in metals or semiconductors. In this paper we present micro-milling results obtained with silicon, using a new version of INO pulsed fiber MOPA laser platform offering programmable pulse amplitude profiles at the nanosecond time scale in two different modes of emission. In a first mode, shaped nanosecond pulses are emitted, whereas shaped bursts of picosecond pulses are emitted in the second mode.

The first objective of the experiments carried out in this work was to explore the potential improvement than can be expected from the burst regime with respect to the nanosecond regime for optimizing laser micro-milling in crystalline silicon, an industrially important material. The material removal efficiency and surface quality were characterized for both modes. For each tested amplitude profile and duration, the burst energy was set to the same value than the corresponding nanosecond pulse. The second objective was to determine the impact of the pulse or burst amplitude profile and duration on the material removal efficiency and surface quality. Although our fiber laser technology allows for it in principle, we did not attempt, at this stage, to find the optimum laser pulse parameters.

2. EXPERIMENTAL SETUP AND METHODOLOGY

2.1 MOPA laser system

The MOPA laser master oscillator architecture is based on the direct modulation of the injection current of a wavelength-stabilized semiconductor laser diode emitting at 1064 nm. The laser uses an embedded digital industrial laser pulse shaping platform allowing for programming pulse shapes easily from a remote computer communicating with the laser. In this platform, called MOPAW (***M**aster **O**scillator with **P**rogrammable **A**rbitrary **W**aveform*), a digital control unit (DCU) and a high-speed digital-to-analog converter (DAC) are used in conjunction to generate a pulse having a predetermined amplitude profile or shape. The DCU generates a waveform by concatenation of consecutive temporal "bins", the amplitude of each "bin" being programmed independently with a 10-bit resolution. Each "bin" has a temporal width of 2.5 ns and 1 to 32 "bins" can be addressed, thus allowing pulse durations in the range of 2.5 ns to 80 ns. Up to 32 different pulse shapes can be stored in memory and pulse-to-pulse shape selection at high repetition rates (up to 1 MHz) is available for processes asking for pulse shaping on demand. A special module allows for choosing between the nanosecond and picosecond burst modes.

The master oscillator output was amplified using three fiber amplifier stages, namely a preamplifier stage, a booster stage and a power amplifier stage. The booster and power amplifier stages employed Yb-doped, polarization maintaining, cladding-pumped large-mode area (LMA) fibers as the gain media. The fibers were designed and fabricated in our facilities, based on INO's proprietary triple clad fiber technology. A special core design allowed for efficiently amplifying high peak power pulses (> 30 kW) while maintaining an excellent beam quality. The large mode field diameters (16 µm for the booster and 24 µm for the power amplifier) also allowed for keeping control over fiber nonlinearities such as stimulated Brillouin scattering (SBS), four-wave mixing (FWM), self-phase modulation (SPM) and stimulated Raman scattering (SRS). The most interesting aspect of this LMA fiber technology is its ability to maintain stable beam characteristics under temperature changes or under thermo-mechanically induced stresses, making it a suitable device for an industrial environment. The MOPA laser system architecture is depicted in Fig. 1. Figure 2 illustrates the picosecond burst shaping mode. In this mode, individual pulses are emitted at a repetition rate of 1.8 GHz within a burst, each pulse having a FWHM duration of 60 ps. Since the pulse shaping time resolution is 2.5 ns, the amplitudes of about 4-5 pulses located within each single temporal "bin" are simultaneously adjusted to the same level when tailoring the burst amplitude profile. In the picosecond burst mode, the peak power typically reaches at least five times the peak power emitted in the nanosecond mode, as shown in figure 3.

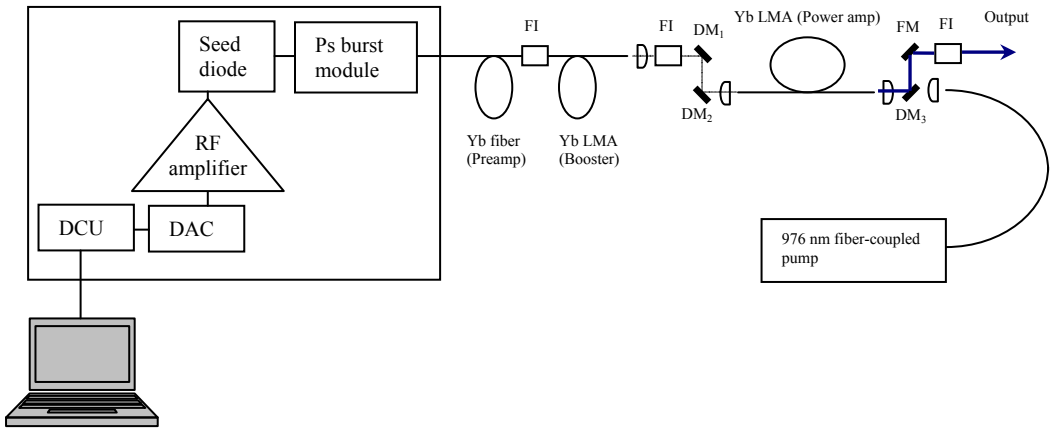

Fig. 1. Schematic view of MOPA laser system (DMx: dichroic mirrors, FM: folding mirror, FI: Faraday isolator).

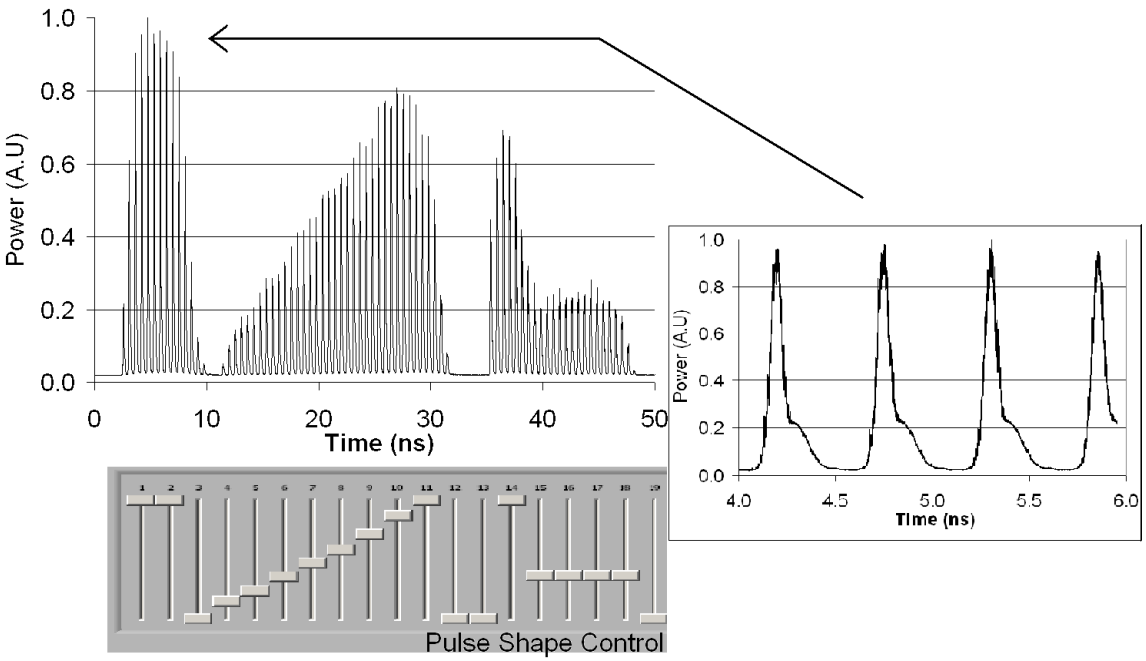

Fig. 2. Picosecond burst shaping mode.

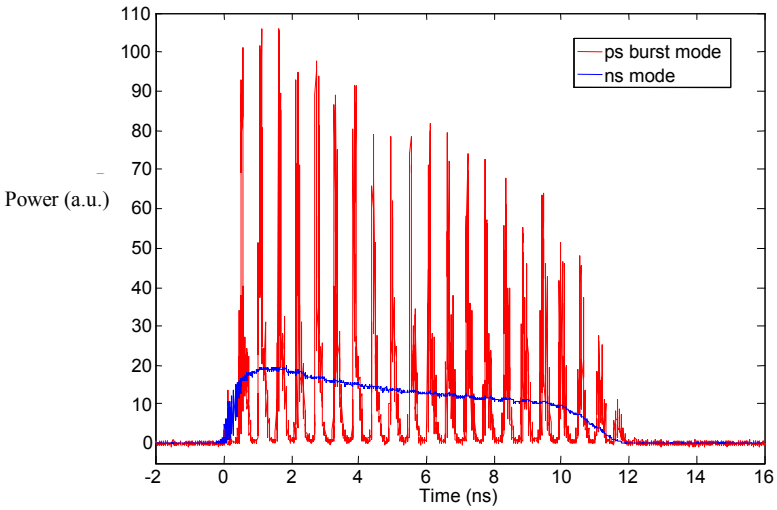

Fig. 3. Peak power in picosecond burst mode vs nanosecond pulse with the same energy .

2.2 Micro-milling setup and methodology

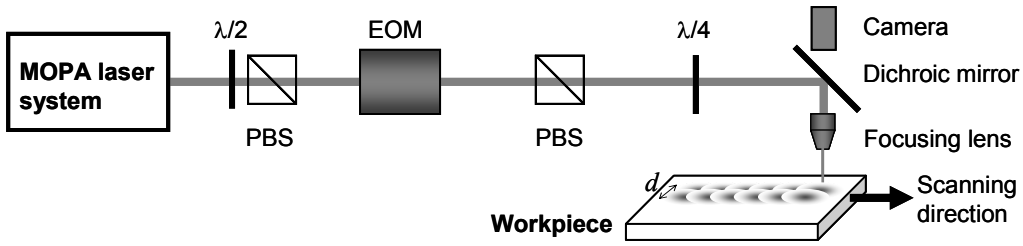

Fig. 4. Experimental setup (PBS: polarizing beamsplitters, EOM: electro-optic modulator)

The focusing lens, as shown in Fig. 4, has a focal length of 38 mm and was chosen long enough to produce a laser spot size almost constant along the total trench depth but small enough to get the necessary power densities for vaporization of the material. The trenches were made by milling several layers in a raster scan fashion. The number of grooves was set to obtain 60-µm wide trenches. No post-processing of the samples other than a simple cleaning with alcohol was done after the laser micro-milling. The pulse-to-pulse overlap C_{p-p} representing the degree of overlapping between the pulses along the scanning direction and the lateral overlap C_l representing the degree of overlapping between the grooves are respectively defined as

$$C_{p-p} = \left(1 - {}^{s_s}\!/_{f_p \phi}\right) \qquad \text{and} \qquad C_l = \left(1 - {}^{d}\!/_{\phi}\right) \tag{1}$$

where s_s is the scanning speed, f_p the repetition rate, ϕ the laser spot diameter, and d is the distance between two consecutive grooves. Values of C_{p-p} and C_l were set to 57% and 48%, respectively, corresponding to the optimal values found for micro-milling of steel and aluminum[3,4]. In our experiments, the laser spot diameter on the target was kept fixed at 14 µm.

The material removal efficiency is defined as the capacity for a laser pulse (of energy E_p) to remove a certain volume of material (V_p). This can be calculated using the following equation:

$$Efficiency = \frac{V_p}{E_p} = \frac{\Delta z_n \cdot s_s \cdot d}{E_p \cdot f_p \cdot n} \quad \left[\mu m^3/\mu J\right], \tag{2}$$

where Δz_n is the total trench depth and n is the number of ablated layers. Because of the speed limitation of our high-precision positioning system to match the high repetition rate of the laser, the desired pulse-to-pulse overlap was obtained by reducing the repetition rate of the pulse train (down to 400 Hz) using an electro-optic modulator combined with a polarizing beamsplitter. To evaluate the removal efficiency for each processed trench, the trench width and trench depth were measured using an optical microscope. Scanning electron microscopy was employed to evaluate the milling quality. For some of the trenches, a confocal laser scanning microscope was used to characterize the average surface roughness.

In the experiments two different energy levels were employed, 5 µJ and 9 µJ. Seven types of pulse shapes were used, with five different pulse durations (2.5,10,20,30 and 40 ns). Table 1 summarizes the key parameters of those pulse shapes. For the 2.5 ns duration only the square pulse shape was available, as this duration corresponds to the pulse shaping resolution in the time domain. For all chair-like shapes, the amplitude ratio of the two plateaus (Min amp/Max amp) was kept constant at 1/3. Micro-milling tests were conducted with all shapes, in the nanosecond mode as well as in the picosecond burst mode.

Table 1. Key parameters of the optical pulse shapes employed in the micro-milling experiments.

Pulse shape	Name	Pulse duration (τ_L), ns	Min amp / Max amp	Duration of Max/ τ_L
	Square	2.5,10,20,30,40	1	1
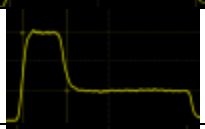	25-75% chair	10,20,30,40	1/3	0.25
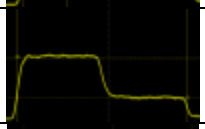	50-50% chair	10,20,30,40	1/3	0.50
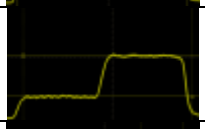	Inverted chair 50-50%	10,20,30,40	1/3	0.50
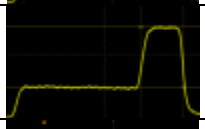	75-25% chair	10,20,30,40	1/3	0.25
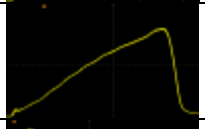	Saw tooth	10,20,30,40	~ 0	---
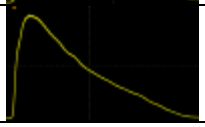	Inverted saw tooth	10,20,30,40	~ 0	---

3. EXPERIMENTAL RESULTS

Fig. 5 and Fig. 6 show the material removal efficiencies obtained at 5 µJ and 9 µJ respectively, for the different pulse shapes and pulse durations. At 5µJ, no ablation was obtained with some of the pulse shapes having durations longer than 20 ns, whereas all shapes at all durations produced ablation at 9 µJ.

Interestingly, the results obtained at 5 µJ in the nanosecond regime can be used to determine the dependency of the laser ablation threshold on the pulse duration. Knowing the laser spot diameter on the target, the maximum intensity (in GW/cm^2) for each pulse can be straightforwardly calculated from the energy per pulse and from the pulse shape. For chair-like and square shapes, the duration of the maximum of intensity vary with the total pulse duration, yielding a data set allowing for evaluating the ablation threshold as a function of the duration of the maximum. The critical intensity at the ablation threshold I_{th} can be estimated using[1]

$$I_{th} \sim \frac{\Omega \rho \sqrt{D}}{(1-R)\sqrt{\tau}} \qquad (3)$$

where Ω is the enthalpy of vaporization per unit of mass, ρ is the density, D is the thermal diffusivity, R is the reflectivity of the target and τ is the laser pulse duration. For silicon Ω =15.63 x 10^3 J/g, ρ = 2.5 g/cm^3 (liquid phase) and D = 0.14 cm^2/s (liquid phase). Fig. 7 shows experimentally determined values of I_{th} from the micro-milling experiments carried out at 5 µJ as a function of the duration of the maximum intensity episode, along with a curve fit based on equation (3).

For the curve fit, the only fitting parameter was R, and the best fit yielded R = 0.29, a typical value for silicon at 1064 nm. As appearing in Fig. 7, good agreement is found between measured and predicted values.

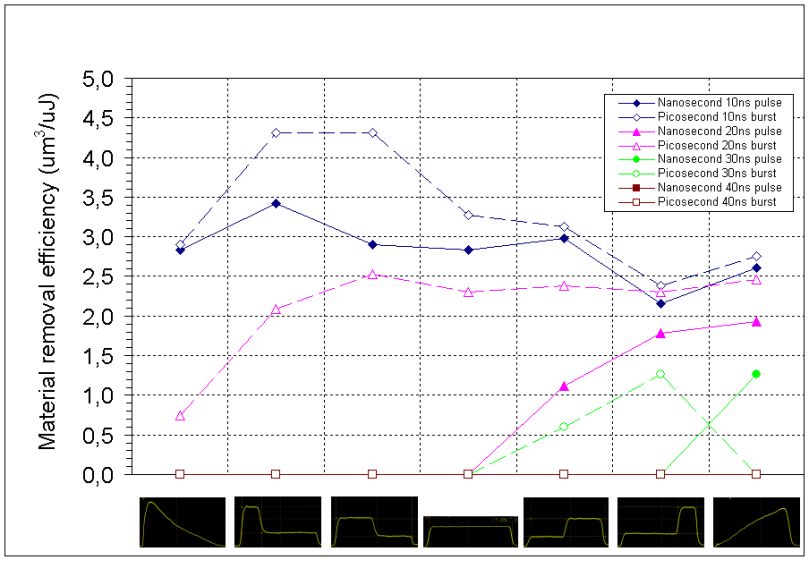

Fig. 5. Material removal efficiency as a function of pulse shape, pulse duration and mode of operation (nanosecond vs picosecond burst), for a pulse (burst) energy of 5 µJ.

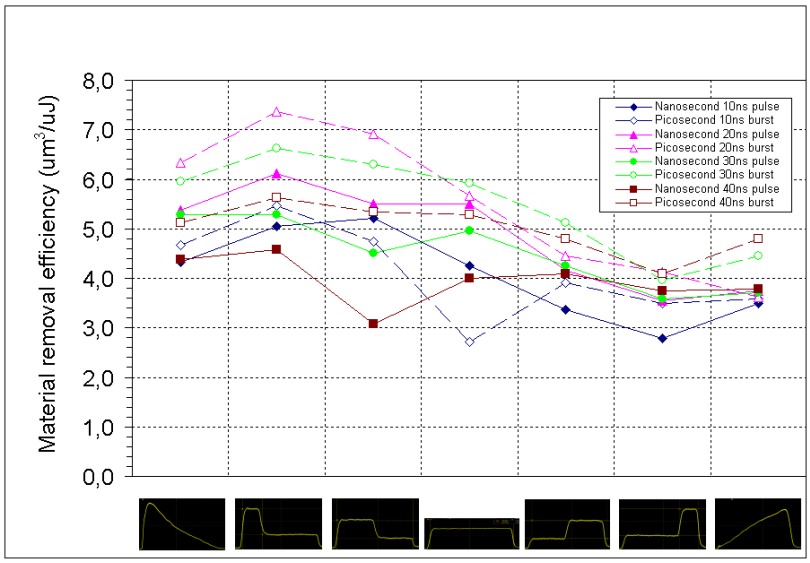

Fig. 6. Material removal efficiency as a function of pulse shape, pulse duration and mode of operation (nanosecond vs picosecond burst), for a pulse (burst) energy of 9 µJ.

Not shown on the graphs of Fig. 5 and Fig. 6 are the removal efficiencies obtained with a 2.5 ns square pulse. All values (5 µJ, 9µJ, nanosecond, picosecond burst) yielded efficiencies in the range of 2.0 to 2.4 $\mu m^3/\mu J$, despite the fact that in all cases the peak intensity (1.34 GW/cm^2, 2.4 GW/cm^2, 11.2 GW/cm^2 and 20 GW/cm^2 for the 5 µJ nanosecond, 9 µJ nanosecond, 5 µJ picosecond burst and 9 µJ picosecond burst respectively) was significantly higher than the threshold intensity appearing in Fig. 7. The shallow heat penetration depth (~0.2 µm) corresponding to the short duration of the

pulse is probably responsible for the limited material removal efficiency. The picosecond burst mode is of no help in that case, the intensities exceeding anyway the reported threshold intensity of ~5-10 GW/cm^2 for plasma ignition in silicon[5].

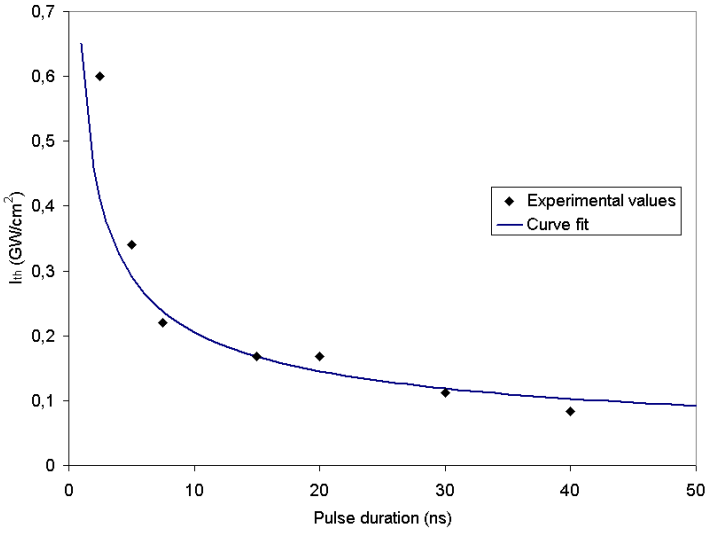

Fig. 7. Threshold laser intensity for ablation as a function of pulse duration.

As appearing in figure 6, the shapes having an energy distribution such that more energy is delivered at the beginning of the pulse than at the end of the same are generally more efficient. This can be understood by considering the time required to produce significant evaporation and the energy and time left for evaporating the material thereafter. The critical time t_{vap} for reaching the vapour phase under a laser intensity I can be estimated using[1]

$$t_{vap} \sim D\left[\frac{\Omega\rho}{(1-R)I}\right]^2 \qquad (4)$$

This time can be calculated for each shape, as well as the energy and time remaining for evaporation. For example, for the 25-75% and 75-25% chair shapes with a pulse duration of 30 ns at 9 µJ in the nanosecond mode the times needed to establish evaporation are 2.7 ns and 22.7 ns respectively. The times left for evaporation are therefore 27.3 ns and 7.3 ns respectively. Further, the energy left for evaporation reach 7.4 µJ for the 25-75% shape whereas it is only 4.4 µJ for the 75-25% chair. Therefore, significantly more energy and more time are available for evaporation with the 25-75% chair shape, compared to the 75-25% chair shape, hence a better removal efficiency with the former (5.29 µm^3/µJ) compared to the later (3.58µm^3/µJ).

Fig. 5 and Fig. 6 also show that in most cases (but not in all cases) the picosecond burst mode increases the material removal efficiency with respect to the nanosecond mode. Fig. 8 illustrates the average improvement (among all tested shapes) obtained as a function of the pulse (burst) duration for the two energy levels employed in our experiments. The best improvement factors (more than 25%) were obtained with the longer pulse durations, probably due to a stronger plasma shielding effect occurring at shorter durations, since the intensity of each picosecond pulse decreases as the burst duration increases for a given energy per burst. For example, with 9 µJ per burst, the maximum intensity varied between 5 and 10 GW/cm^2 among the shapes, with an average of 8.6 GW/cm^2, which is sufficient to establish plasma and the associated shielding effects[5]. The fact that similar improvement levels can be obtained with shorter bursts when lowering the energy per burst from 9 µJ to 5 µJ is also consistent with the plasma shielding assumption. Fig. 9 gives the absolute value of the average material removal efficiency in both modes as a function of the pulse (or burst) duration, with 9 µJ per pulse (or burst). Interestingly, the best improvement factors are obtained for those pulse durations that also give the best absolute efficiencies (durations longer than 10 ns).

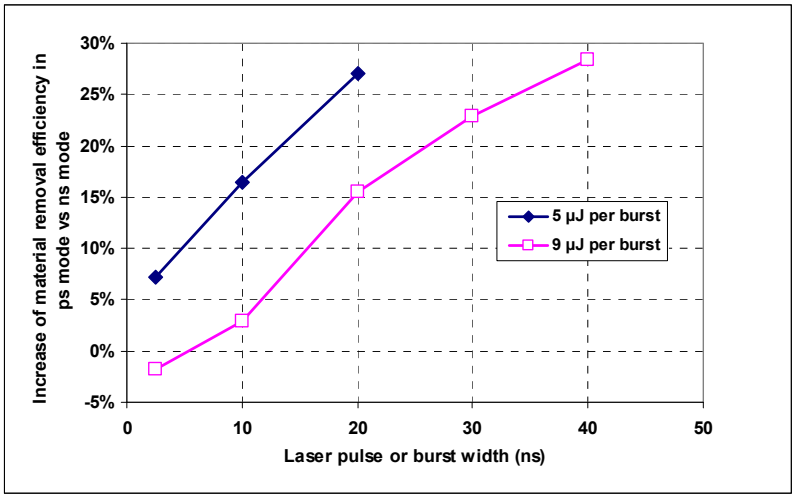

Fig. 8. Improvement of material removal efficiency in the picosecond burst mode with respect to the nanosecond mode, as a function of the pulse (or burst) width.

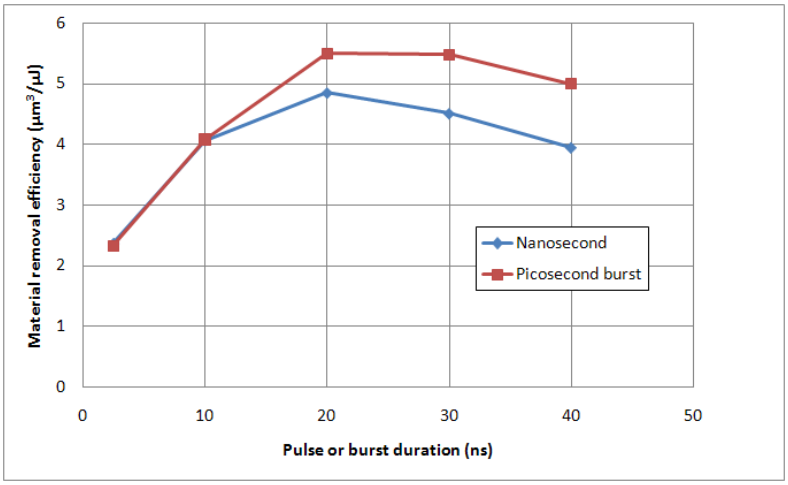

Fig. 9. Absolute value of the average material removal efficiency in nanosecond mode vs picoseconds burst mode as a function of the pulse (or burst) duration. Energy per pulse (or burst): 9 µJ .

Fig. 10 illustrates the measured improvement of the surface roughness for different pulse shapes, energy per pulse and pulse durations. Although an improvement is noticed for most shapes (up to 25%), in some cases the roughness significantly degrades when employing the picosecond burst mode. The degradation is observed for pulse durations of 10 ns and 20 ns. For the 25-75% chair shape the quality degrades at 5 µJ and at 9 µJ, whereas for the shape 75-25% the degradation is observed at 9 µJ only. Fig. 11 shows SEM images of trenches micro-milled with that same 75-25% chair shape at 9 µJ, as a function of the pulse (or burst) duration for both modes of operation of the laser. For the 20 ns duration the sharp transition appearing in the SEM image for the nanosecond mode is an artefact. With burst durations of 30 ns or 40 ns in the picosecond burst mode, the material removal efficiency *and* the surface quality S_a were better than any result obtained in the nanosecond mode with the same pulse shape. The degradation of the surface quality observed with shorter pulse durations (e.g. < 20 ns) in the picosecond burst mode is consistent with similar observations reported in the literature[5] for the medium high intensity regime (5-20 GW/cm^2).

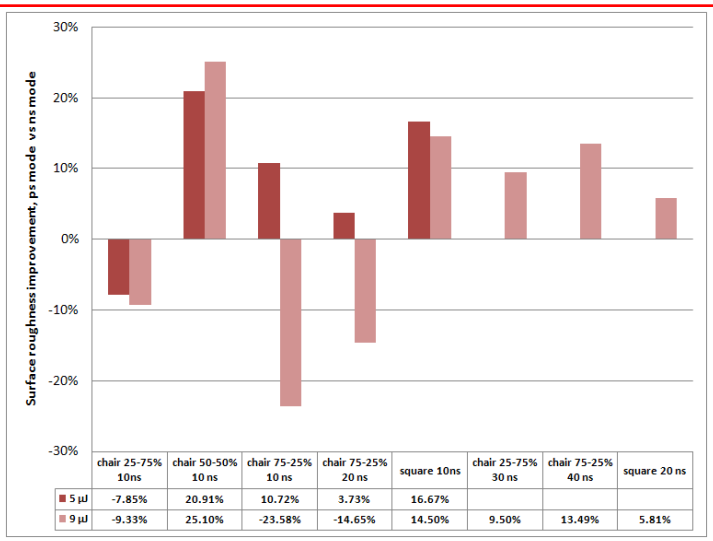

	chair 25-75% 10ns	chair 50-50% 10 ns	chair 75-25% 10 ns	chair 75-25% 20 ns	square 10ns	chair 25-75% 30 ns	chair 75-25% 40 ns	square 20 ns
5 µJ	-7.85%	20.91%	10.72%	3.73%	16.67%			
9 µJ	-9.33%	25.10%	-23.58%	-14.65%	14.50%	9.50%	13.49%	5.81%

Fig. 10. Improvement of surface roughness obtained with the picosecond burst mode compared to the nanosecond mode.

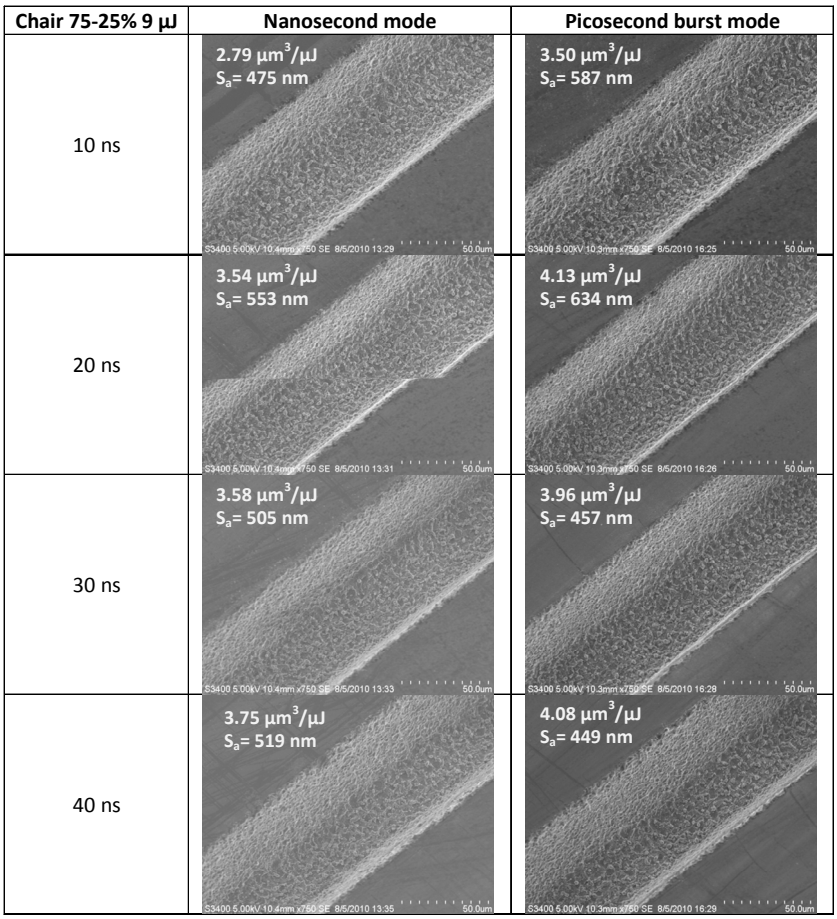

Fig. 11. SEM images of micro-milled trenches obtained with the 75-25% chair shape at 9 µJ in the nanosecond mode and in the picosecond burst mode.

4. CONCLUSIONS

The different results obtained in the micro-milling experiments carried out in this work demonstrate the usefulness of agile pulsed laser sources providing straightforward control over the pulse characteristics (temporal shape, duration, energy) in the nanosecond mode as well as in the picosecond burst mode. Our results show that the pulse shaping can be advantageously used to develop laser micro-milling processes offering the best conditions for the process throughput or for the surface quality, as both aspects were found to be sensitive to the pulse shape. Moreover, we showed that the laser flexibility can be advantageously used to test theoretical models or assumptions about the physical mechanisms that dominate the laser-matter interaction, such as the dependency of the critical laser intensity at the ablation threshold with respect to the pulse duration. Improvement of up to 25% in the material removal rate and on the surface roughness were obtained with the picosecond burst mode with respect to the nanosecond mode, keeping the total energy per pulse (or bust) constant. The improvement was observed for burst durations longer than 20 ns, below which plasma shielding effects limits the efficiency and the surface quality.

REFERENCES

[1] Chichkov, B.N., Momma, C., Nolte, S., von Alvensleben, F., Tünnermann, A., “Femtosecond, picosecond and nanosecond laser ablation of solids”, Appl. Phys. A 63, 109-115 (1996).
[2] Hu, W., Shin, Y.C., King, G.,”Modeling of multi-burst mode picosecond laser ablation for improved material removal rate”, Appl. Phys. A 98, 407-415 (2010).
[3] Deladurantaye, P., Gay, D., Cournoyer, A., Roy, V., Labranche, B., Levesque, M., Taillon, Y., “Material micromachining using a pulsed fiber laser platform with fine temporal nanosecond pulse shaping capability”, Proc. SPIE 7195, art. no. 71951S (2009).
[4] Gay, D., Cournoyer, A., Deladurantaye, P., Briand, M., Roy, V., Labranche, B., Levesque, M., Taillon, Y., “Micro-milling process improvement using an agile pulse-shaping fiber laser”, Proc. SPIE 7386, art. no. 73860R (2009).
[5] Ren, J., Orlov, S.S., Hesselink, L., Howard, H., Conneely, A., “Nanosecond laser silicon micromachining”, Proc. SPIE 5339, 382-393 (2004).